Sensors and Materials, Vol. 17, No. 8 (2005) 441–451
MYU Tokyo

S & M 0622

Determination of Thermal Expansion Coefficient of Thermal Oxide

Chingfu Tsou*, Yu-Sheng Huang, Hung-Chung Li and Teng-Hsien Lai

Department of Automatic Control Engineering, Feng Chia University,
Taichung, Taiwan

(Received December 5, 2004; accepted September 13, 2005)

Key words: thermal expansion coefficient, thermal oxide film, microbridge, buckling deformation, finite element analysis

An accurate thermal expansion coefficient (α) of a thin film is important in the design of microelectronic devices and microsystems. In this research, we present the use of microbridge buckling deformation caused by residual stresses to determine the α of a thermal oxide (SiO_2) film. The determination of α is supported through experimental means and the analysis by finite-element method (FEM) of the buckling profiles of a microbridge. Moreover, to obtain the α of a thermal SiO_2 film accurately, a nanoindentation system and an optical microscope with a high-resolution gauge were used to determine the elastic modulus of the thermal SiO_2 film and the α of the silicon substrate, respectively. By combining micro-electro-mechanical systems (MEMS) technologies and FEM with thermo-mechanical analysis, the α of the thermal SiO_2 film was calculated. The measured α of the thermal SiO_2 film at room temperature is 0.24×10^{-6}/°C with a standard deviation of 0.02×10^{-6}/°C.

1. Introduction

The mechanical thermal properties of thin films are important parameters in the design of both microelectronic devices and microsystems, particularly in the areas of IC packaging and the fabrication of thermally driven microactuators or thermal microsensors. Physically, the functional performance of those microdevices is affected directly by the thermal expansion coefficient (α) of a thin film.[1–6] However, the thermal expansion coefficient of thin films approximately 1 μm thick or less can be significantly influenced by their fabrication processes.[7,8] To properly design microelectronic devices as well as micromachined components, it is necessary to characterize the thermal expansion coefficient of thin-film materials.

*Corresponding author, e-mail address: cftsou@fcu.edu.tw

Several measurement techniques including X-ray diffraction analysis,[9,10] the use of optically levered laser beams,[11,12] and the deformation of suspended micromachined structures[7,13,14] have been applied to the measurement of the thermal expansion coefficient of thin films. As described in refs. 9–12, these methods are used to determine film stress by measuring the changes in wafer curvature induced by the deposited films, and hence thermal expansion coefficient can be extracted. However, X-ray diffraction analysis is only suitable for measuring crystalline structures, and the technique using an optically levered laser beam requires knowledge of the thermal expansion coefficient of the substrate and the elastic modulus of a thin film. In the case of using the deformation behavior of a micromachined structure to determine the thermal expansion coefficient of a thin film, such as microcantilever bending and microring or micromembrane buckling mentioned in refs. 7, 13 and 14, these methods are only suitable for characterizing CMOS intermetal dielectric and metal films to be utilized in micro-electro-mechanical systems because both the fabrication processes and the micromachined structure used in those studies are simplified. However, the problem with the micromachined structure test is that the changes in the measured magnitude of the out-of-plane deformation determined using optical interferometric techniques are affected by the thermal creep of a thin film.

In this paper, a microbridge fabricated using a standard bulk micromachining process is presented to determine the thermal expansion coefficient of a thin film. According to ref. 15, by the first approximation, residual stresses in a thin film as shown in Fig. 1 can be regarded as

$$\sigma_{\text{total}} \approx \sigma_0 + \sigma_1\left(\frac{2y}{h}\right), \tag{1}$$

where h is the thickness of the thin film and $y \in (-h/2, h/2)$ is the coordinate across the thickness with its origin at the midplane of the film. From eq. (1), residual stresses are composed of a mean component, σ_0, and a gradient component, σ_1. The bending of the microcantilever is caused by gradient residual stress as shown in Fig. 2(a). On the other hand, the buckling of the microbridge, as shown in Fig. 2(b), is induced by the mean compressive residual stress. Therefore, through an experimental process, the out-of-plane deformation of these microstructures can be measured using optical interferometrics. After that, by comparing the results of experimental measurements and finite-element method (FEM) simulations, film residual stresses can be determined.

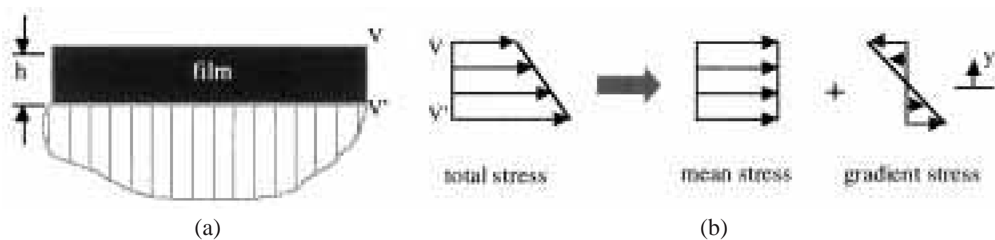

(a) (b)

Fig. 1. (a) Schematic diagram of film on substrate and (b) distribution of residual stresses on cross section A-A'.

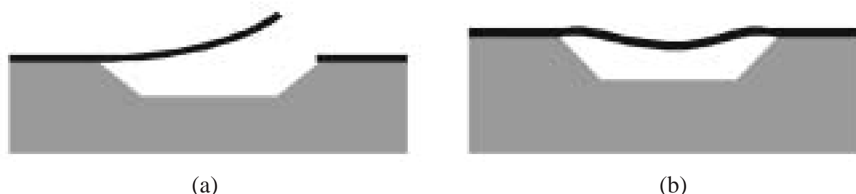

(a) (b)

Fig. 2. Out-of-plane deformations: (a) microcantilever bending; and (b) microbridge buckling.

During the thermal growth of an amorphous dielectric film, the mean residual stress σ is generated by the mismatch $\Delta\alpha$ between the film and the substrate. In the case of a uniaxial sample, thermal stress is given by

$$\sigma = E\Delta\alpha\Delta T, \tag{2}$$

where E is the film's elastic modulus. Since the temperature change ΔT in the microfabrication process can be marked, and the elastic modulus of the thin film is known, the average $\Delta\alpha$ over the process range can be calculated using the measured value of residual stresses. Thus, the thermal expansion coefficient of the thin film can be extracted using the known thermal expansion coefficient of the substrate. For a microbridge with compressive residual stress to have sufficient buckling, a thermal SiO_2 film was used as a thin-film test structure in this study. To eliminate the error margin of material correlation parameters while implementing thermal stress analysis, in this study, we use a nanoindenation system and an optical microscope to determine the elastic modulus of the thermal SiO_2 film and the thermal expansion coefficient of the silicon substrate, respectively.

2. Experiments

To accurately measure the thermal expansion coefficient of a thermal SiO_2 film, the experiments in this study include primarily three tasks: (1) Determine the elastic modulus of the thermal SiO_2 film using the nanoindenation technique, and then use this measured value as a data point in calculating gradient residual stress. (2) Fabricate a micromachined test structure using a bulk micromachining process and then measure the out-of-plane deformation magnitude using interferometric profilometry to determine the residual stress. (3) Use an optical microscope to observe the heated silicon substrate and to obtain the thermal expansion coefficient of silicon. Note that the test specimens for all experiments are fabricated by the same oxidation process. In the following, the detailed content of each experiment is described.

2.1 *Elastic modulus of* SiO_2

Experiments to measure the elastic modulus of a 1-µm-thick thermal SiO_2 film grown on (100) silicon wafers were performed using a commercial nanoindention system with a 0.0002 nm displacement theoretical resolution and a 1 nN force resolution. A Berkovich indenter with a triangular pyramidal tip was used in this experiment. During the thin-film indentation test, a commercial indentation system was used to continuously record the load

and displacement of the indenter head.

In this experiment, a series of ten tests on a single sample were performed. The measured elastic moduli of the thermal SiO_2 film at different indentation depths are shown in Fig. 3. The elastic modulus changed markedly in the beginning due to the surface profile of the indentation point. The elastic modulus varies with indentation depth owing to the substrate effect. An approximate rule of thumb is that the depth of the contact should be less than 10% of the film thickness, although in some materials, some claims of depths of up to 25% have been made.(16) Thus, in agreement with that mentioned previously, the elastic modulus of SiO_2 under consideration is 72.2±2.5 GPa at 5% and 10% of the film thickness.

2.2 *Beam deformation*

The effect of residual stress on the micromachined test structure was investigated in this experiment. A SiO_2 microcantilever and a SiO_2 microbridge 1 μm thick, 10 μm wide, and 20–140 μm long were fabricated by a standard bulk micromachining process. First, a (100) single-crystal Si substrate was placed in a furnace at 1050°C for 150 min to grow a thermal oxide layer 1 μm thick. After the oxide layer was patterned, the substrate was etched anisotropically using KOH. The test beams were all released from the substrate after being etched for 30 min. However, due to the influence of the etching selectivity of KOH, the measured thickness of the suspended microcantilever and microbridge was 0.98 μm.

A scanning electron microscopy (SEM) image of a typical microbridge is shown in Fig. 4. The microbridge buckles downward because of compressive residual stress. To determine the effect of residual stresses on the micromachined test structure, the out-of-plane deformation of different beams was measured by noncontact interferometric profilometry. The out-of-plane deflection profile of the microbridge shown in Fig. 5(b) was measured along line AA’ in Fig. 5(a). Hence, the maximum deflection amplitude of the beam at point C was determined. The measured deformation amplitude of a microbridge of different lengths *L* is shown in Fig. 6. The data points in Fig. 6 denote the average values of the measured upward buckling deformation for ten different arrays.

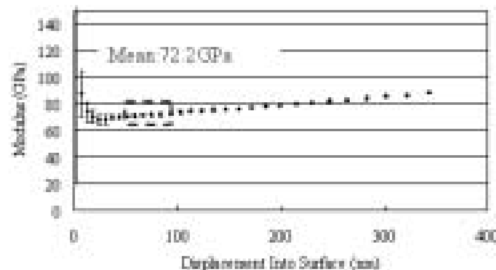

Fig. 3. Elastic moduli of thermal SiO_2 film at different indentation depths.

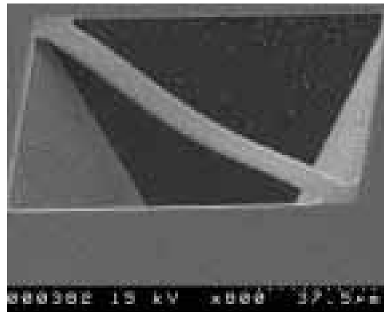

Fig. 4. SEM image of microbridge fabricated in this study.

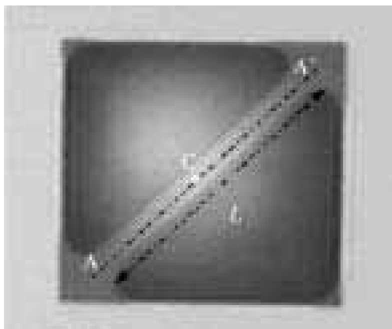

(a)

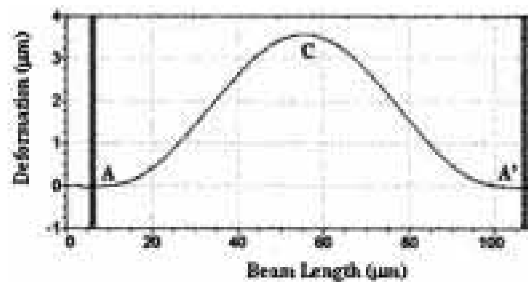

(b)

Fig. 5. Optical microscopy photograph of SiO_2 microbridge to be measured and (b) measured deflection profile of beam shown in (a) along path A-C-A'.

In addition, using the above-mentioned measurement method, the deflection profile of microcantilevers was also measured as shown in Fig. 7. The deflection profile of the microcantilever gradually increases as beam length increases since the beam was bent by gradient residual stress. Therefore, with a change in out-of-plane deformation along the beam length, the radius of curvature of the microcantilever was obtained automatically from measurement software. The average measured value for several microcantilevers with a beam length of 100 μm and width of 10 μm was 3.26 mm.

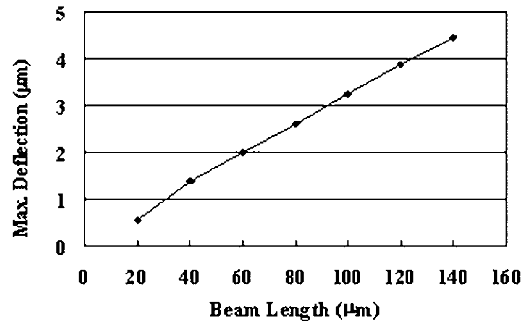

Fig. 6. Measured deflection amplitudes of SiO_2 microbridge vs beam length.

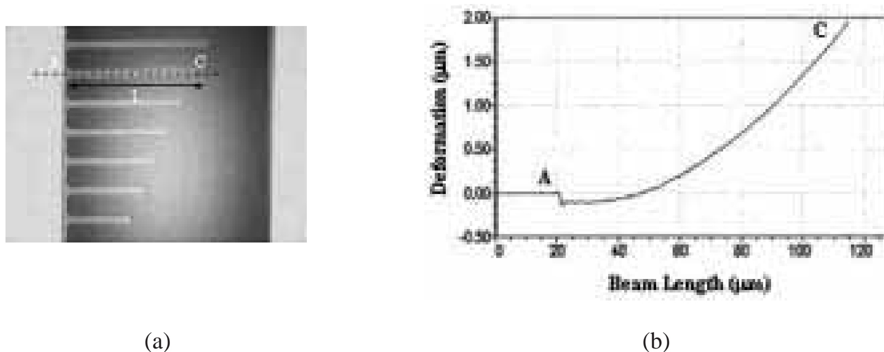

(a) (b)

Fig. 7. Optical microscopy photograph of SiO_2 microcantilever to be measured and (b) measured deflection profile of beam shown in (a) along path A-C.

2.3 *Thermal expansion coefficient of Si*

To stop the parameters of the reference material from producing an error margin in the analyzing process, in this study, we measured the thermal expansion coefficient of the silicon substrate. This experiment was designed to directly cut a wafer into a rectangular sample 2 cm × 0.8 cm in size and then, using a diamond pen, to engrave two parallel caves on the rectangular sample. The distance between these two caves can be treated as an equivalent length to be used as reference value when measuring thermal expansion coefficient. Then, the sample was heated on a heating stage, which had a controller to maintain deviations in temperature to within 0.1°C. An optical microscope with a 0.1 µm resolution for height position was used to observe the equivalent length change of the sample. In dilatometry, the linear thermal expansion coefficient α is given by

$$\alpha(T) = \left(\frac{\Delta L}{L}\right)\left(\frac{1}{\Delta T}\right), \tag{3}$$

where L is the sample's original length (at room temperature), T is the sample's temperature and ΔL is the change in the sample's length due to the change in its temperature ΔT. Consequently, according to the above eq. (Eq. 3) and the results measured, the linear thermal expansion coefficient of the silicon substrate was determined to be 2.67×10^{-6}/°C at a temperature of 25°C.

3. Analysis and Discussion

In this research, we used the out-of-plane buckling behavior of a microbridge to calculate thin-film mean compressive residual stress. In addition, the thermal expansion coefficient of a thin film was determined using thermal stress analysis. Gradient residual stress can be regarded as being caused by localized effects including interstitial or substitutional defects and atomic peening, and mean residual stress can be regarded as being caused by a mismatch in thermal expansion coefficient between the film and the substrate. In this section, the out-of-plane deformation caused by mean stress and gradient stress on a microbridge is studied. In addition, the deformation amplitudes of the microbridge caused by various mean compressive stresses are predicted using FEM.

3.1 *Gradient residual stress*

In the film fabrication, gradient residual stress causes microcantilever deformation. However, the peak gradient residual stress can be found by measuring the curvature of a microcantilever and is given by[17]

$$\sigma_1 = \frac{Eh}{2R}, \tag{4}$$

where R is the radius of curvature of the microcantilever. Correspondingly, substituting the actual thickness h (0.98 μm) of the microcantilever and its elastic modulus E (72.2 GPa) measured by the indentation test as well as the radius of curvature R (3.26 mm) into the eq.,[4] the calculated peak value of the gradient residual stress of the thermal SiO_2 film is determined to be approximately 10.85 MPa. This gradient stress σ_1 may be used as an initial loading condition for FEM followed by thermomechanical analysis.

3.2 *Mean residual stress*

The nonlinear analysis by FEM was used to simulate the buckling behavior of a microbridge caused by mean compressive stress, in that the applied residual stress can cause a temperature effect on the film. Consequently, the out-of-plane deformation configuration of the microbridge resulting from residual stresses can be predicted and characterized. From this experiment, a constant stress gradient can be extracted using the radius of curvature of the microcantilever. Therefore, in the following buckling simula-

tion, the applied residual stresses superpose the effects using various mean residual stresses and the measured constant stress gradient.

A two-dimensional model as shown in Fig. 8 was established to simulate the microbridge and its boundaries. The triangular marker in the diagram and its sets indicate that the microbridge boundary is fixed on the surface of the silicon substrate. The initial temperature of the film material is T_0. However, the residual stresses of eq. (1) in this model, based on eq. (2), can be represented by the following eq. and simulated by the temperature effect.

$$\sigma_{\text{total}} \approx E\alpha\left[\left(\frac{T_1+T_2}{2}-T_0\right)+\left(\frac{T_1-T_2}{2}\right)\left(\frac{2y}{h}\right)\right], \text{ if } T_2 > T_1 \tag{5}$$

Thus, by setting any fictitious mechanical parameters (such as: $E = 70$ GPa, $\alpha = 0.25\times10^{-6}$/°C) in the FEM model and applying the temperature effect (T_1 and T_2) to simulate the residual stresses acting on the microbridge, the variation in the out-of-plane deflection along the beam length with induced thermal stress can be obtained. The typical nonlinear FEM result for the buckled microbridge of thickness $h = 0.98$ μm and beam length $L_e = 100$ μm is shown in Fig. 9. Figure 9 (a) shows that the microbridge buckled upward after being subjected to a constant total residual stress. Figure 9 (b) shows the variation in the maximum out-of-plane deflection of the microbridge with the applied mean compressive stress contributed by a loading condition of a constant stress gradient with a peak value of 10.85 MPa. This figure acts as a calibration curve for the calculated thermal expansion coefficients of SiO_2. Thus, according to the simulation shown in Fig. 9 (b) in comparison with the experiment result shown in Fig. 6 under the same deformation of 3.24 μm, the extracted mean residual stress is 180 MPa. With all measured experimental results being substituted into eq. (2) of the thermal stress analysis, the thermal expansion coefficient of thermal SiO_2 of 0.24×10^{-6}/°C was obtained.

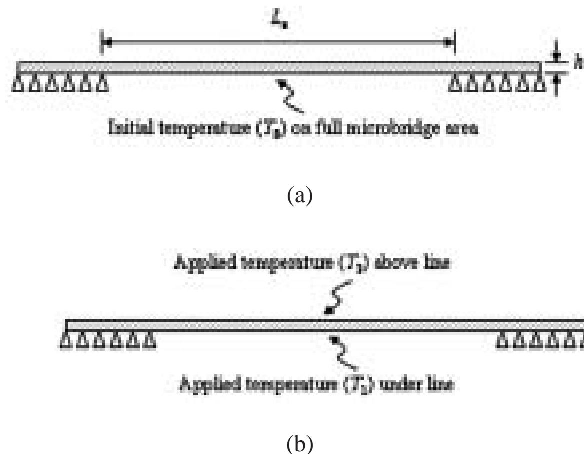

Fig. 8. The two-dimensional analysis model with (a) initial boundary conditions and (b) applied temperature effect established in this study.

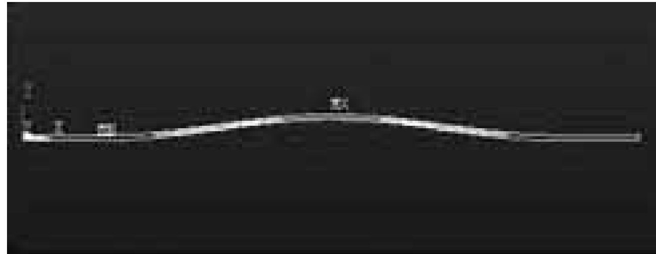

(a)

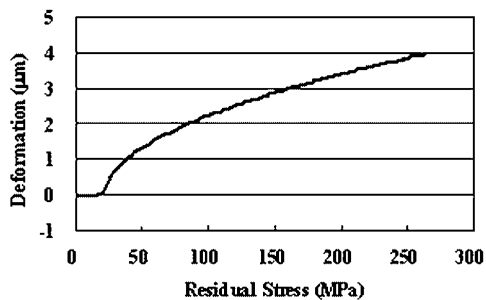

(b)

Fig. 9. FEM analysis result: (a) microbridge buckled upward after being subjected to both mean and gradient stresses, and (b) variation in maximum out-of-plane deflection with total stress acting on midplane of film.

According to these measurements, microbridges of lengths L = 60 μm, 80 μm, 100 μm, 120 μm, and 140 μm were also analyzed in this study. Figure 10 shows the variation in microbridge length with the $\Delta\alpha$ calculated from eq. (2). It is obvious that the variation in α mismatch with beam length L is a state value for the longer beam. However, the shorter beam can be affected more significantly by its boundary imperfections caused by undercut etching, and it is not suitable for beam theory analysis.[17,18] On the other hand, a reliable and accurate α mismatch in this experiment should be considered from the longer beam because of its approach to a constant value. Therefore, considering the microbridges of lengths L = 100 μm, 120 μm, and 140 μm, the calculated thermal expansion coefficient of a thermal SiO_2 film at room temperature is 0.24×10^{-6}/°C with a standard deviation of 0.02×10^{-6}/°C. The value obtained in previous study[19] is approximately 0.55×10^{-6}/°C. However, this value will vary depending on how the oxide was produced and what measurement techniques were used.

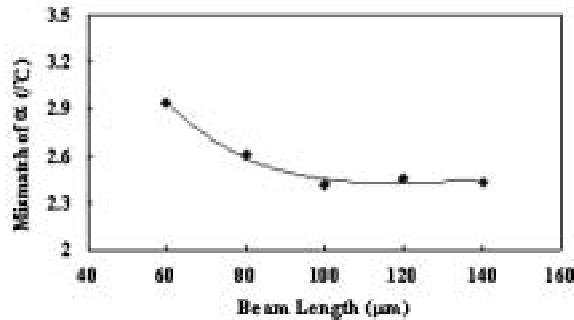

Fig. 10. Variation in α mismatch with microbridge length *L*.

4. Conclusions

In this study, the use of microbridge buckling deformation in extracting the thermal expansion coefficient of a thin film is demonstrated. Both experimental and FEM approaches were used to determine the thermal expansion coefficient of a thermal SiO_2 film. In addition, the elastic modulus of a thermal SiO_2 film and the thermal expansion coefficient of silicon were also measured in this experiment to eliminate the error margin of related material parameters in thermal mechanical analysis. The thermal expansion coefficient of thermal oxide at room temperature was determined to be 0.24×10^{-6}/°C with a standard deviation of 0.02×10^{-6}/°C. More importantly, the measurement mechanism presented here can also be applied to the measurement of other thin films or used as a test key for characterizing CMOS intermetal dielectric films, however, only under the condition that the films are limited to a compressive prestress.

Acknowledgements

This project was (partially) supported by the National Science Council of Taiwan under grant of NSC-92-2218-E-035-012. The authors would also like to thank the NSC Central Regional MEMS Center (Taiwan), the Nano Facility Center of National Tsing Hua University, the Precision Instrument Support Center of Feng Chia University, and the NSC National Nano Device Laboratory (NDL) for providing the fabrication facilities.

References

1 M. Tagami, H. Ohtake, Y. Hayashi and H. Miyamoto: International Interconnect Technology Conference 2003 (IEEE, San Francisco, 2003) p. 213.
2 A. S. Chen, L. T. Nguyen and S. A. Gee: Effect of material interactions during thermal shock testing on IC package reliability, Components, Hybrids, and Manufacturing Technology (IEEE, Orlando, 1993) p. 614.

3 Y. Wang, X. Cui and W. Wu: Solid-State and Integrated-Circuit Technology 2001 (IEEE, Shanghai, China, 2001) p. 109.
4 H. K. Eron, J. R. Richard and T. A. Gregory: Solid-State Sensors and Actuators and Eurosensors IX 1995 (IEEE, Stockholm, Sweden, 1995) p.154.
5 O. Paul, M. von Arx and H. Baltes: Solid-State Sensors and Actuators and Eurosensors IX 1995 (IEEE, Stockholm, Sweden) p.178.
6 P. Norlin, O. Ohman, B. Ekstrom and L. Forssen: Solid-State Sensors and Actuators 1997 (IEEE, Chicago, 1997) p. 507.
7 W. Fang, H. C. Tsai and C. Y. Lo: Sens. Actuators, A **77** (1999) 21.
8 W. Fang and C. Y. Lo: Sens. Actuators, A **84** (2000) 310.
9 D. N. Batchelder and R. O. Simmons: J. Chem. Phys. **41** (1964) 2324.
10 D. N. Batchelder and R. O. Simmons: J. Appl. Phys. **36** (1965) 2864.
11 S. P. Murarka and T. F. Retajczyk Jr.: J. Appl. Phys. **54** (1983) 2069.
12 T. F. Retajczyk Jr. and A. K. Sinha: Appl. Phys. Lett. **36** (1980) 161.
13 T. Kramer and O. Paul: Sens. Actuators, A **92** (2001) p. 292.
14 V. Ziebart, O. Paul and H. Baltes: MRS Proc. **546** (1999) 103.
15 W. Fang and J. A. Wickert: J. Micromech. Microeng. **6** (1996) 301.
16 G. M. Pharr and W. C. Oliver: MRS Bull. **7** (1992) 28.
17 S. Timoshenko and S. Woinowsky-Krieger: Theory of Plates and Shells (McGraw-Hill, New York, 1959).
18 W. Fang and J. A. Wickert: J. Micrimech. Microeng. **4** (1994) 116.
19 G. Carlotti, P. Colpani, D. Piccolo, S. Santucci, V. Senez, V. Senez, G. Socino and L. Verdini: Thin Solid Films **414** (2002) 99.